Journal of Sound and Vibration (2002) **249**(2), 325–349
doi:10.1006/jsvi.2001.3832, available online at http://www.idealibrary.com on IDEAL®

ACTIVE CONTROL OF SOUND TRANSMISSION THROUGH A CURVED PANEL INTO A CYLINDRICAL ENCLOSURE

J. K. Henry and R. L. Clark

Department of Mechanical Engineering and Materials Science, Duke University, Box 90300, *Durham, NC* 27708-0300, *U.S.A.*

(*Received* 27 *December* 1999, *and in final form* 17 *May* 2001)

Current research has focused on the reduction of sound transmission through the aircraft fuselage into the interior of aircraft due to turbulent boundary layer excitation. The present work utilizes an analytical model, previously developed by the authors, as a design tool in the development of feedback control systems to attenuate sound transmission. The model is of a typical aircraft panel in service conditions with attached piezoelectric actuators, coupled to the interior acoustics of a rigid-wall cylinder. The control design process, which includes transducer optimization and $\mathscr{H}_2$ synthesis, is documented. Control designs are presented utilizing both acoustic pressure measurements and structural velocity measurements. Results indicate that an active structural acoustic control design using structural velocity measurements and insight gained from analysis of the structural acoustic coupling can achieve performance similar to a control design utilizing acoustic pressure measurements. Further analysis shows that the active structural acoustic control design can be implemented regardless of panel position on the enclosure, and can withstand perturbations in panel dynamics resulting from variations in static pressure loading with flight altitude. Significant reduction of sound transmission into the enclosure is achieved.

1. INTRODUCTION

When an aircraft flies through air, a turbulent boundary layer is created on the exterior of the fuselage, exciting the individual fuselage panels. In turn, the vibrating panels generate an undesired acoustic response inside the fuselage. Since the turbulent boundary layer excitation is stochastic, traditional feedforward techniques for reduction of sound radiation from the fuselage panels that require a reference signal correlated with the disturbance are not practical. As a result, current research has focused on the use of feedback control for the reduction of noise transmission into the enclosure. Researchers have sought to adapt many of the control techniques developed to reduce the radiation of flat plates into acoustic space [1–8] to the problem of noise transmission into the fuselage of an aircraft. Efforts in this direction began with feedback control of the radiation of a flat panel into a rectangular enclosure [9–13]. Research by the authors seeks to extend this effort to the feedback control of radiation from a curved panel into a cylindrical enclosure.

Knowledge of the application physics of the system being controlled is vital to the design and implementation of feedback control systems. Previous research by the authors has resulted in the development of an analytical model of a typical fuselage panel in service conditions [14, 15]. Recent research by the authors analyzed the structural acoustic coupling between a typical fuselage panel and a cylindrical enclosure [16]. The current

0022-460X/02/020325 + 25 $35.00/0

paper utilizes the analytical model of the coupled structural acoustic system and insight gained from the analysis of the structural acoustic coupling to design feedback control systems to reduce noise transmission from typical fuselage panels into a cylindrical enclosure. The design process documented herein includes transducer size and placement optimization, and employs $\mathscr{H}_2$ control design techniques. The resulting feedback control designs presented use either acoustic pressure measurements or structural velocity measurements as performance metrics. Results indicate that the structural velocity measurements can be weighted according to the maximum structural acoustic coupling coefficients for each structural mode to create a structural acoustic control system that performs as well as a control system utilizing acoustic pressure measurements. The structural acoustic control system presented is implemented on typical fuselage panels at various positions on the cylindrical enclosure in order to demonstrate that the performance is unaffected by panel position. Finally, the structural acoustic control system is shown to achieve significant performance despite small perturbations in static pressure loading with varying flight altitude, and to remain stable for larger perturbations.

2. MODEL DEVELOPMENT

In this section, the equations of motion of a curved panel and a cylindrical enclosure are presented first, followed by the definition of simulation parameters for a typical aircraft panel and fuselage. Then, the structural acoustic coupling between the panel and enclosure is discussed briefly. Based on the analysis of the structural acoustic coupling, the system models are simplified to facilitate control design. Finally, the two-port control problem is introduced and formulated for the curved panel system.

2.1. SYSTEM EQUATIONS OF MOTION

Consider a rigid-wall cylindrical enclosure with rigid endcaps excited by the vibrations of a curved panel mounted just inside the boundary of the cylinder, with the co-ordinate system shown in Figure 1. The acoustic response within the cavity is given by

$$\{\ddot{\phi}^c\} + [\mathbf{\Omega}^2]\{\phi^c\} = c^2 S_0 [\mathbf{\Lambda}]^{-1} [\mathbf{C}]\{\dot{\mathbf{q}}\}, \tag{1}$$

where ϕ^c is the cavity velocity potential, $\mathbf{\Omega}^2$ is the diagonal matrix of the natural frequencies of the cavity squared, c is the speed of sound in the cavity, S_0 is the surface area of the curved panel, $\mathbf{\Lambda}$ is a diagonal matrix of the modal volumes, $\mathbf{C}$ is the matrix of structural acoustic coupling coefficients and $\mathbf{q}$ is the vector of generalized displacements of the curved panel.

The equations of motion of a curved panel, as shown in Figure 2, with shear-diaphragm boundary conditions subjected to transverse loading from an attached piezoelectric actuator, static pressure loading from a pressure differential across the panel, acoustic pressure loading from the cavity acoustic field, and a modal disturbance approximating turbulent boundary layer excitation are

$$[\mathbf{M}_s + \mathbf{M}_p]\{\ddot{\mathbf{q}}\} + [\mathbf{K}_s + \mathbf{K}_p + \mathbf{K}_{tf}]\{\mathbf{q}\} = [\mathbf{\Theta}]^{\mathrm{T}}\{\mathbf{v}\} - \rho_0 S_0 [\mathbf{C}^{\mathrm{T}}]\{\dot{\phi}^c\} + [\mathbf{B}_f + \mathbf{P}_f]\{\mathbf{f}\}, \tag{2}$$

where $\mathbf{M}_s$ and $\mathbf{K}_s$ are the structural mass and stiffness matrices respectively; $\mathbf{M}_p$ and $\mathbf{K}_p$ are the piezoelectric mass and stiffness matrices respectively; $\mathbf{K}_{tf}$ is the stiffness matrix resulting from the pressure differential, $\mathbf{\Theta}$ is the electromechanical coupling matrix, $\mathbf{v}$ is the vector of

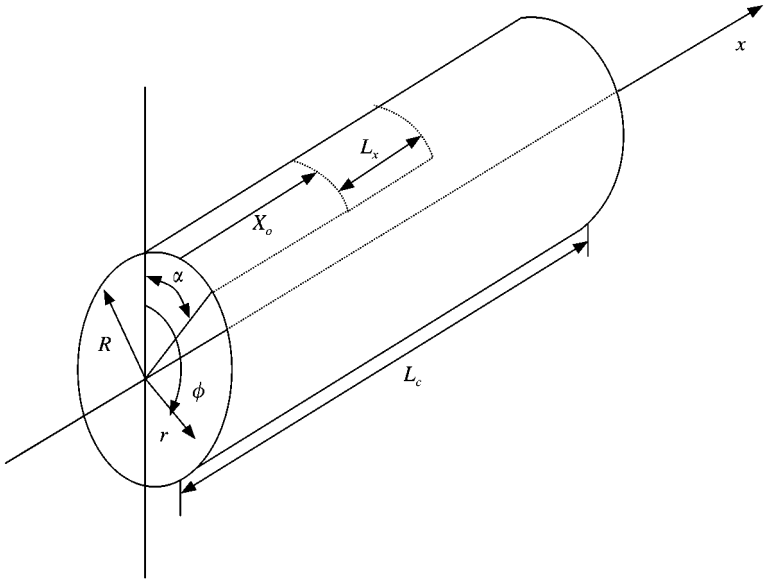

Figure 1. Co-ordinate system of rigid-walled cylinder with endcaps (not shown) and curved panel mounted just inside boundary.

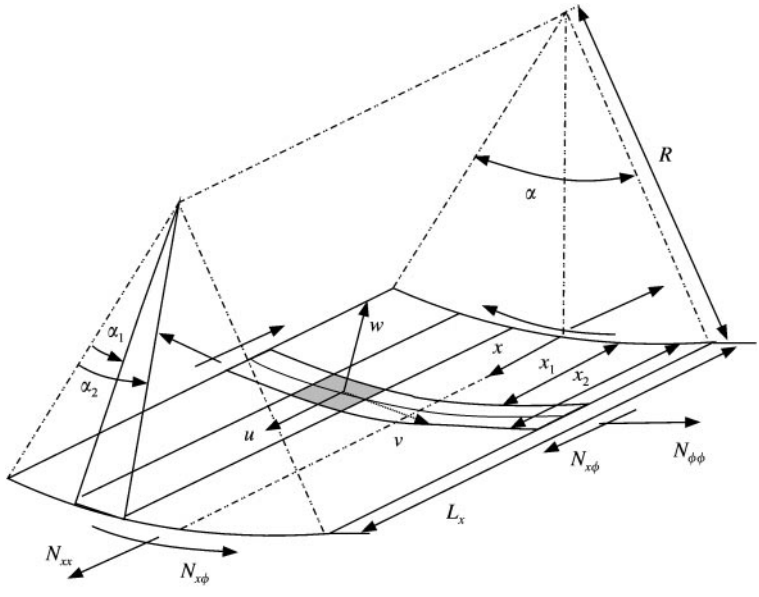

Figure 2. Co-ordinate system of curved panel with example of attached piezoelectric transducer.

generalized co-ordinates associated with the voltage applied to the piezoelectric actuator, ρ_0 is the density of the air in the enclosure, $\mathbf{B}_f$ is the generalized modal disturbance force, and $\mathbf{P}_f$ is the generalized static pressure force.

A detailed derivation of these equations of motion is available in references [14–17]. The block diagram of the coupled structural acoustic system is shown in Figure 3.

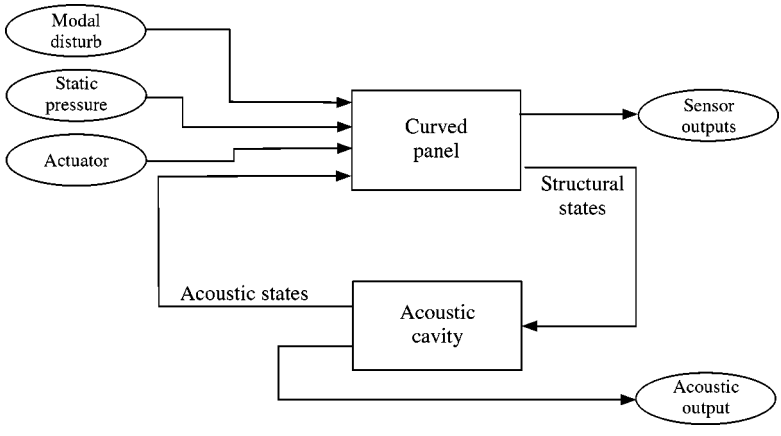

Figure 3. Block diagram of coupled system.

2.2. SIMULATION PARAMETERS

The dimensions of the curved panel considered in this investigation have been selected to approximate fuselage sub-panels found on a Boeing 737. Unless otherwise noted, the following parameters for the curved panel are held fixed throughout the investigation: $L_x = 0{\cdot}508\,\text{m}$, $R = 1{\cdot}75\,\text{m}$, $\alpha = 0{\cdot}131\,\text{rad}$, $h_s = 1{\cdot}8\,\text{mm}$, $E_s = 69{\cdot}3 \times 10^9\,\text{N/m}^2$, $\rho_s = 2680\,\text{kg/m}^3$, $v_s = 0{\cdot}33$. The panel is centered 30% down the length of the cylinder, such that $x_0 = 0{\cdot}3L_c - (L_x/2)$. It is placed circumferentially starting at $\phi = 0$.

The dimensions of the rigid-walled cylinder have also been selected to approximate the size of the fuselage of a Boeing 737. The cylinder and the contained air have the following parameters: $L_c = 43{\cdot}18\,\text{m}$, $R = 1{\cdot}75\,\text{m}$, $\rho_0 = 1{\cdot}21\,\text{kg/m}^3$, $c = 343\,\text{m/s}$. The cylinder is assumed to have internal pressure corresponding at atmospheric pressure at 10,000 ft, and to be in a medium with external pressure corresponding to atmospheric pressure at 40,000 ft. Thus, the curved panel is subjected to a static pressure load resulting from the differential.

2.3. STRUCTURAL ACOUSTIC COUPLING

The structural acoustic coupling coefficients describe the interaction between the acoustic modes of the enclosure and structural modes of the curved panel system, such that

$$\mathbf{C} = \frac{1}{S_0} \int_{S_0} \mathbf{\Psi}(x, \phi)\, \mathbf{\Gamma}(R, \phi, x)\, \mathrm{d}S_0, \tag{3}$$

where $\mathbf{\Psi}$ and $\mathbf{\Gamma}$ are the mode shape functions for the structural modes of the curved panel and the acoustic modes of the cylindrical enclosure respectively. Analysis of the structural acoustic coupling coefficients between the structural modes of the typical aircraft panel below 1000 Hz and the acoustic modes of the cylindrical enclosure was presented in reference [16]. Analysis showed that predominately axial, low order structural modes couple most efficiently to the acoustic modes of the enclosure. The maximum structural acoustic coupling coefficients between the structural modes below 1000 Hz and acoustic

TABLE 1

Maxima of the normalized coupling coefficients for structural modes

Structural mode (p, n)	Structural wavenumber (1/m)	Max of normalized coup. coeff.	Acoustic mode (β, τ, μ)	Acoustic wavenumber (1/m)	Structural natural freq. (Hz)	Acoustic natural freq. (Hz)
(1, 1)	27·7	0·803	(0, 1, 81)	5·9	338·3	321·7
(2, 1)	31·5	0·783	(0, 1, 115)	8.4	437.0	456·8
(3, 1)	35·7	0·462	(0, 1, 140)	10·2	561·2	556.0
(4, 1)	39.7	0·084	(0, 1, 183)	13·3	695·1	726·8
(1, 2)	39·9	0·137	(20, 1, 0)	12·7	699·2	693·1
(2, 2)	41·2	0·099	(19, 1, 105)	14·3	747·9	781·4
(3, 2)	43·5	0·064	(17, 1, 160)	16·0	833·0	871·2
(5, 1)	43·9	0·195	(0, 1, 210)	15·3	847·6	834·1
(4, 2)	46·5	0·029	(14, 1, 215)	18·1	952·4	988·7

modes proximal in natural frequency for the system described above are listed in Table 1 where β, τ, and μ are the circumferential, radial, and axial modal indices respectively. The investigation indicated that the (1,1), (2,1), (3,1), (4,1), (1,2) and (5,1) structural modes couple most efficiently to the modes of the enclosure. Furthermore, analysis showed that the structural modes which couple most efficiently to the modes of the enclosure are the same regardless of the position of the panel on the cylindrical enclosure. Also, due to high acoustic modal density and the size of the panel, the position of the panel on the cylindrical enclosure does not significantly affect the maximum structural acoustic coupling coefficient for each structural mode. The insight provided by this analysis is important for the subsequent active structural acoustic control design. Since the predominately axial, low order structural modes couple most efficiently to the axial acoustic modes of the enclosure and very inefficiently to the circumferential acoustic modes of the enclosure in the bandwidth of concern, the acoustic system can be approximated by a 1-D model, including only the axial modes, in the control design process. The objective to the control system will be to reduce the excitation of the axial acoustic modes of the enclosure by the structural modes, resulting in the reduced contribution of the axial acoustic modes to the overall acoustic response in the cavity.

With the intention of further simplifying the coupled system, the effects of the acoustic pressure loading on the panel can be investigated. Consider the coupled structural acoustic system previously described with a secondary curved panel, with the same dimensions as the typical fuselage panel, centered 70% down the length of the cylinder and positioned circumferentially starting at $\phi = 0$. Assume the secondary curved panel is loaded only by the acoustic pressure in the cavity created by the vibration of the primary curved panel positioned at the other end of the cylindrical enclosure and subjected to a modal disturbance input. Figure 4 compares the frequency response from the modal disturbance input to the piezoelectric sensor on the primary curved panel with the frequency response from the modal disturbance on the primary panel to the piezoelectric sensor on the secondary panel. As the figure indicates, the response of the secondary panel due to the acoustic loading is several orders of magnitude less than the response of the primary panel due to the modal disturbance. Note also that the "rippling" observed in the frequency response of the secondary panel at low frequency results from the response of individual acoustic modes of the cylinder (the acoustic modal density is lower at these frequencies, and the excited acoustic modes are more dependent on panel position) excited by the

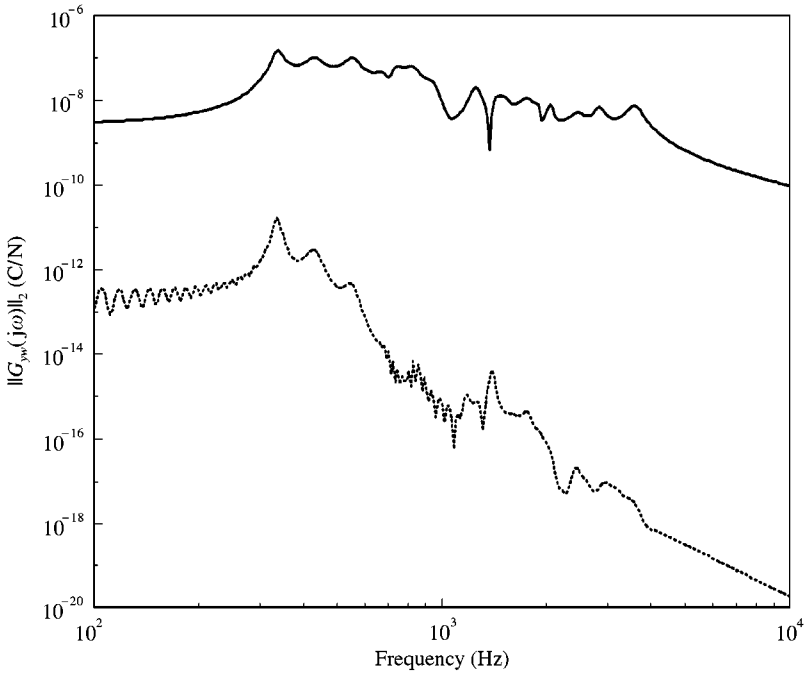

Figure 4. Comparison of the frequency response from the modal disturbance to the piezoelectric sensor of the vibrating curved panel with the frequency response from the modal disturbance of the vibrating panel to the piezoelectric sensor on the secondary panel: ——, primary panel; – – – – –, secondary panel.

low-frequency response of the primary panel. This response is typical of secondary panels at other positions on the cylinder. Therefore, since each panel on the fuselage is subjected to modal disturbance loading representing the turbulent boundary layer excitation, the acoustic feedback path is insignificant. As a result, the acoustic feedback from one structural panel to another or from a panel to itself can be neglected in the control system design process. The coupled system can be simplified by neglecting the acoustic feedback path and using the cavity model as a "radiation filter" of sorts to determine the effects of the control system on radiation into the cavity.

2.4. TWO-PORT PROBLEM FORMULATION

For the purposes of control design, the curved panel system can be stated in standard two-port problem format:

$$\begin{bmatrix} \mathbf{z}(s) \\ \mathbf{y}(s) \end{bmatrix} = \begin{bmatrix} \mathbf{P}_{zw}(s) & \mathbf{P}_{zu}(s) \\ \mathbf{P}_{yw}(s) & \mathbf{P}_{yu}(s) \end{bmatrix} \begin{bmatrix} \mathbf{w}(s) \\ \mathbf{u}(s) \end{bmatrix}, \tag{4}$$

where $\mathbf{z}(s)$ is the vector of error outputs, $\mathbf{y}(s)$ is the vector of measured outputs, $\mathbf{w}(s)$ is the vector of exogenous inputs, and $\mathbf{u}(s)$ is the vector of control inputs. The system matrix, $\mathbf{P}(s)$, is partitioned according to the input–output variables. For the curved panel system, the error outputs are the out-of-plane modal velocities, the measured output is the output of the piezoelectric sensor, the exogenous inputs are the inputs from the static pressure and modal

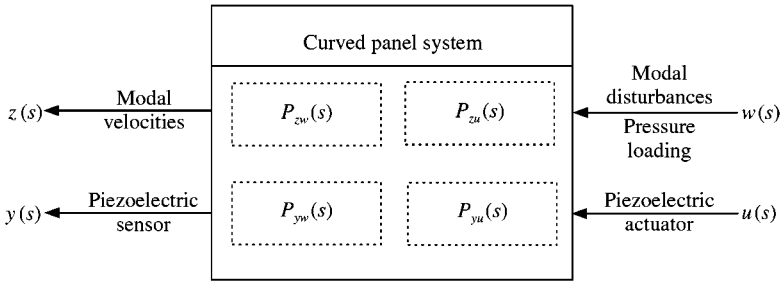

Figure 5. Block diagram of two-port representation of curved panel system.

disturbance loadings, and the control input is the input of the piezoelectric actuator. The system transfer matrix of the curved panel system is created by transforming the equations of motion and output equations into a state-space formulation, and implementated in MATLAB. Figure 5 shows a block diagram of the curved panel two-port system.

3. ACTUATOR PLACEMENT OPTIMIZATION

To allow the compensator to focus control energy on the predominately axial, low order modes of the curved panel, the piezoelectric sensor and actuator sizes and positions are optimized using a method introduced by Clark and Cox [18] and refined by Smith and Clark [19]. This method determines the optimal control actuator and sensor size and placement from a given set of candidate pairs using Hankel singular values of the open-loop controllability and observability Grammians as an optimization metric. The Hankel singular values provide a measure of the degree of coupling between the structural modes and the piezoelectric transducers. The optimization metric developed by Clark and Cox emphasizes coupling to modes within the bandwidth of control, but penalizes coupling to modes outside of this bandwidth. Thus, the method loop-shapes the spatial compensator to provide roll-off outside of the desired control bandwidth. Beyond considering in-bandwidth and out-of-bandwidth modes, the metric developed by Smith and Clark selects modes for control and penalizes modes not considered important for performance, both in-bandwidth and out-of-bandwidth, such that

$$\tilde{J}_{qp} = \frac{\bar{J}^{c}_{qp}}{\bar{J}^{nc}_{qp}}, \tag{5}$$

where $\bar{J}^{c}_{qp}$ is the coupling measure and $\bar{J}^{nc}_{qp}$ is the de-coupling measure of the qth sensor and the pth actuator in the candidate set. The coupling measure for this metric is written over all modes as

$$J^{c}_{qp} = \sum_{i=1}^{I} \kappa_i \left(\frac{\gamma^4_{y_p u_q i}}{\bar{\gamma}^4_{yui}} \gamma^4_{zwi} \right), \tag{6}$$

where γ is the Hankel singular value for the particular input/output path, and κ is a binary vector of length N. Modes to be controlled have an element value of 1 in κ. The de-coupling metric over all modes is written as

$$J^{nc}_{qp} = \sum_{i=1}^{I} (\sim \kappa)_i \left(\frac{\gamma^4_{y_p u_q i}}{\bar{\gamma}^4_{yui}} \gamma^4_{y_p u_q i} \right), \tag{7}$$

TABLE 2

Set of piezoelectric transducer sizes used in the optimization algorithm

Length in x (in)	Length in ϕ (in)
1	1
1	2
2	1
2	2
4	6
6	4
2	6
6	2
1	6
6	1
10	6

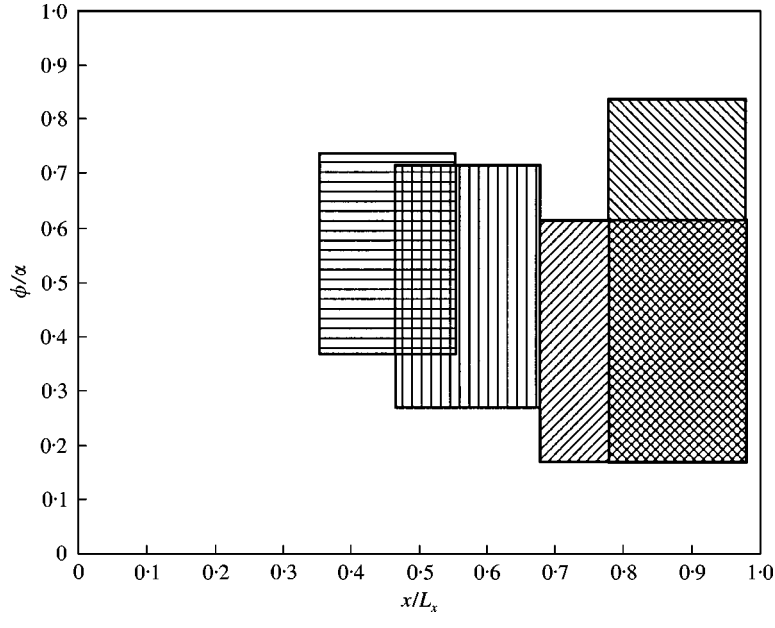

Figure 6. Piezoelectric transducer pair locations on typical fuselage panel: ▧, optimal actuator; ▨, optimal sensor; ▤, arbitrary actuator; ▥, arbitrary sensor.

where the $\sim$ operator is the *one's compliment*, or binary NOT. The actuator and sensor pair which maximize the metric are the optimal transducers demonstrating strong coupling to the selected modes and little coupling to unselected modes and out-of-bandwidth dynamics.

The analysis of the structural acoustic coupling coefficients identified the following structural modes as those with significant coupling to the acoustic modes of the interior: (1,1), (2,1), (3,1), (4,1), (1,2), and (5,1). The κ vector was defined to weight only these desired

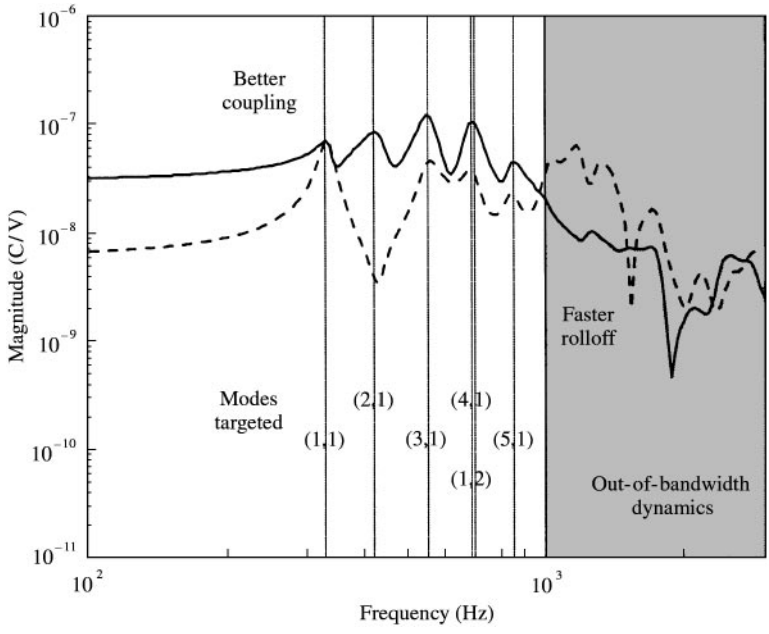

Figure 7. Comparison of the frequency responses for the optimal and arbitrary transducer pairs from actuator to sensor: ——, optimal; – – – – –, arbitrary.

modes in the performance path, $\mathbf{P}_{zw}(s)$. The optimization method was applied for the piezoelectric transducer sizes listed in Table 2 at hundreds of arbitrary placements on the curved panel. The resulting optimal piezoelectric actuator and sensor size and locations are shown in Figure 6. The optimal actuator is a $\mathbf{4} \times \mathbf{6}$ in patch ($0{\cdot}102 \times 0{\cdot}152$ m) centered at $x = 0{\cdot}878L_x$ and $\phi = 0{\cdot}503\alpha$. The optimal sensor is a $\mathbf{6} \times \mathbf{4}$ in ($0{\cdot}152 \times 0{\cdot}102$ m) patch centered at $x = 0{\cdot}898L_x$ and $\phi = 0{\cdot}392\alpha$. Reciprosity and symmetry apply, meaning that the optimal sensor and actuator are interchangeable, and their placements could be simultaneously mirrored across both centerlines. Figure 7 compares the frequency responses from sensor to actuator of the optimal actuator and sensor pair and an arbitrary actuator and sensor pair (refer to Figure 6). The frequency response of the optimal transducer pair demonstrates coupling to the selected curved panel modes and roll-off outside of the bandwidth of control. The frequency response of the arbitrary pair shows coupling only to a few of the selected modes and significant coupling to the out-of-bandwidth dynamics. The advantages of the optimal transducer pair over the arbitrary pair will be exploited in the subsequent control design.

4. CONTROL SYSTEM DESIGN

The controller design is performed using the $\mathscr{H}_2$ feedback control design method [20]. By augmenting the curved panel plant in two-port format, the generalized plant system can be formulated for the $\mathscr{H}_2$ controller design problem [20]. A block diagram of the generalized plant system is shown in Figure 8. The weighting filters in the generalized plant are used to modify the objective and aggressiveness of the controller. The process noise filter, $\mathbf{W}(s)$, is used to shape the disturbance acting on the curved panel system, $w_p(s)$, and is weighted relative to the sensor noise filter. For the purpose of this investigation, the process noise

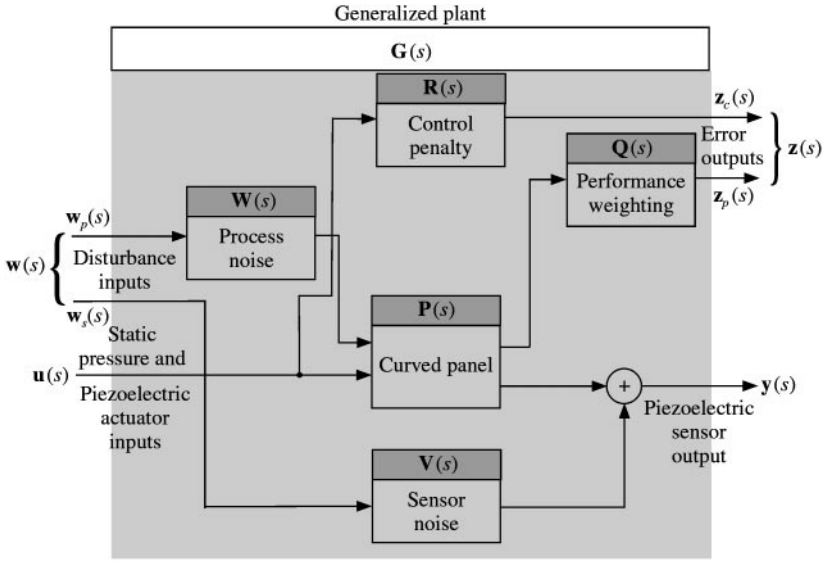

Figure 8. Block diagram of the generalized plant.

filter has unity gain over all frequencies, defining a broader bandwidth of excitation than typically observed in turbulent boundary layer noise. The sensor noise filter, $\mathbf{V}(s)$, is used to define a constant noise level below which the dynamics of the system are not well measured. Since the transducer optimization produced roll-off in the out-of-bandwidth response, a constant gain sensor noise filter can be used to concentrate control effort on the low order, axial panel modes that have responses exceeding the noise level on the sensor. The sensor noise filter can be utilized further to regulate the aggressiveness of the control law and the stability of the closed-loop system. The frequency response of the sensor noise filter is compared to the typical fuselage panel frequency response from the disturbance to the piezoelectric sensor for each of the subsequent control designs. The control penalty filter, $\mathbf{R}(s)$, restrains the input control energy to the curved panel. In this investigation, it is a constant gain filter weighted relative to the different performance weighting filters. The performance weighting filter, $\mathbf{Q}(s)$, is used to define the performance variables to be minimized by the control law. The typical fuselage panel modal velocities are processed by the performance weighting filter in two ways. In the first case, the 1-D cavity model, with the typical fuselage panel modal velocities as inputs, is used as the performance weighting filter to form the simplified coupled system. The performance variables of the generalized plant in this case are the acoustic metric outputs of the 1-D cavity model, which are defined as the pressure contributions of the axial acoustic modes at 100 arbitrary points within the cavity. Thus, the control system is designed based on the dynamics of the simplified coupled system. In the second case, the performance weighting filter is defined to weight the typical fuselage panel modal velocities according to the maximum structural acoustic coupling coefficient between each structural mode and the acoustic modes proximal in natural frequency. The performance variables of the generalized plant in this case are the weighted structural modal velocities. Therefore, the control system is designed based only on the dynamics of the typical fuselage panel system using insight gained from the analysis of the structural acoustic coupling coefficients.

The dynamic response of the resulting generalized plant can be expressed in state-space form:

$$\begin{Bmatrix} \dot{\mathbf{x}}(t) \\ \mathbf{z}(t) \\ \mathbf{y}(t) \end{Bmatrix} = [\mathbf{G}] \begin{Bmatrix} \mathbf{x}(t) \\ \mathbf{w}(t) \\ \mathbf{u}(t) \end{Bmatrix}, \tag{8}$$

where $\mathbf{x}(t)$ is the vector of the states of the generalized plant system, $\mathbf{z}(t)$ is the vector of error outputs, $\mathbf{y}(t)$ is the vector of measured outputs from the piezoelectric sensor, $\mathbf{G}(s)$ is the generalized plant transfer matrix,

$$\mathbf{G}(s) = \left[\begin{array}{c|cc} \mathbf{A} & \mathbf{B}_w & \mathbf{B}_u \\ \hline \mathbf{C}_z & \mathbf{0} & \mathbf{D}_{zu} \\ \mathbf{C}_y & \mathbf{D}_{yw} & \mathbf{0} \end{array}\right], \tag{9}$$

$\mathbf{w}(t)$ is a vector of zero-mean, white-noise processes, $w_p(t)$ and $w_s(t)$, such that the spectral density matrix $\mathbf{S}_{ww}(\mathrm{j}\omega) = \mathbf{I}$ for all ω, and $\mathbf{u}(t)$ is the vector of control inputs from the piezoelectric actuator and the static pressure load. The components of the generalized plant transfer matrix are determined from the combined dynamics of the curved panel two-port system and the aforementioned weighting filters [20].

The cost function to be minimized is the square of the $\mathscr{H}_2$ norm:

$$J = \| \mathbf{T}_{zw} \|_2^2, \tag{10}$$

where $\mathbf{T}_{zw}$ is the closed-loop transfer matrix between the disturbance inputs, $\mathbf{w}(s)$, and the error outputs, $\mathbf{z}(s)$.

5. FEEDBACK CONTROL RESULTS

The generalized plant system was implemented in MATLAB, and the control system design was performed using the μ-Analysis and Synthesis Toolbox [21]. The first case considered is the compensator design using the pressure contributions of the axial acoustic modes at 100 arbitrary points within the cavity as performance metrics. The sensor noise filter is a constant gain filter with magnitude 7×10^{-8}, and is compared to the frequency response of the typical fuselage panel from the modal disturbance to the piezoelectric sensor in Figure 9. The control effort penalty is a constant gain filter with magnitude 1×10^{-4}. The performance weighting filter is the 1-D cavity model including axial acoustic modes below 1400 Hz with the structural modal velocities as inputs and pressure contributions at 100 points distributed throughout the cylinder as outputs for the cost function. The compensator is designed using the generalized plant system and based upon the performance weighting filter, serves to minimize an estimate of the acoustic potential energy of the enclosure. The frequency response of the compensator is shown in Figure 10.

The closed-loop system is formed as shown in Figure 11. The loop is closed around the curved panel system between the sensor output and the actuator input. The two-port model of the curved panel is augmented using redundant input/output paths to create a disturbance to performance path representative of the dynamics of the actuator to sensor path, as shown by the inclusion of $\mathbf{w}_u(s)$ and $\mathbf{z}_y(s)$ in Figure 11. A third output, $\mathbf{z}_u(s)$, is created to allow analysis of the control input signal energy to the curved panel. Additionally, the 1-D cavity model is included as a radiation filter to form the simplified

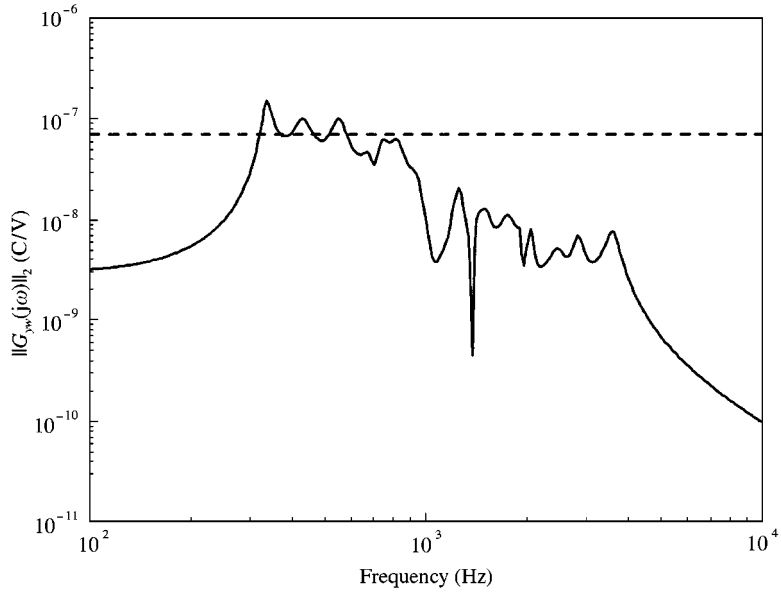

Figure 9. Frequency response of typical fuselage panel from disturbance to sensor compared with sensor noise: ——, $\| G_{yw_p} \|_2$; -----, $\| G_{yw_s} \|_2$.

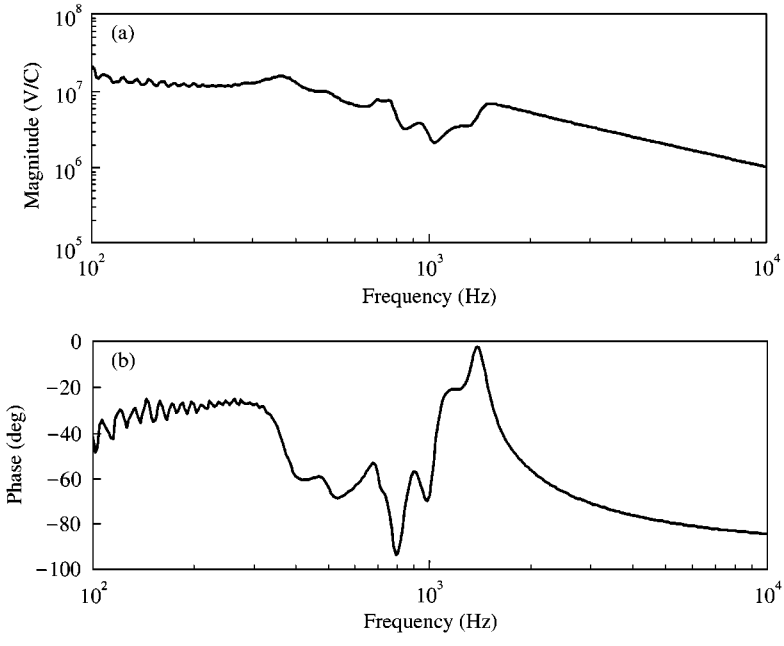

Figure 10. Frequency response of compensator designed using acoustic pressure measurements as performance metrics.

coupled system and to create an acoustic pressure performance metric, $\mathbf{z}_a(s)$, allowing analysis of the impact of the control system on radiation into the cavity. The loop-gain of the system, $\mathbf{K}(s)\mathbf{P}_{yu}(s)$, is shown in Figure 12. The magnitude of the loop-gain of the system does not exceed unity, guaranteeing stability of the closed-loop system over all frequencies

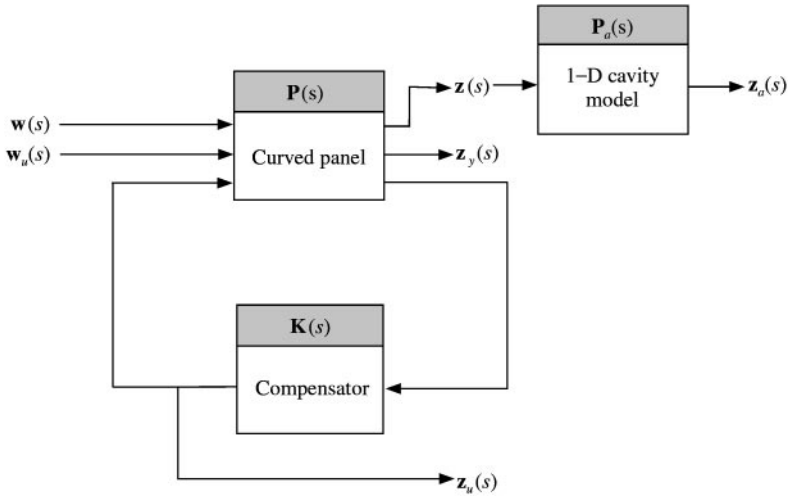

Figure 11. Block diagram of closed-loop system.

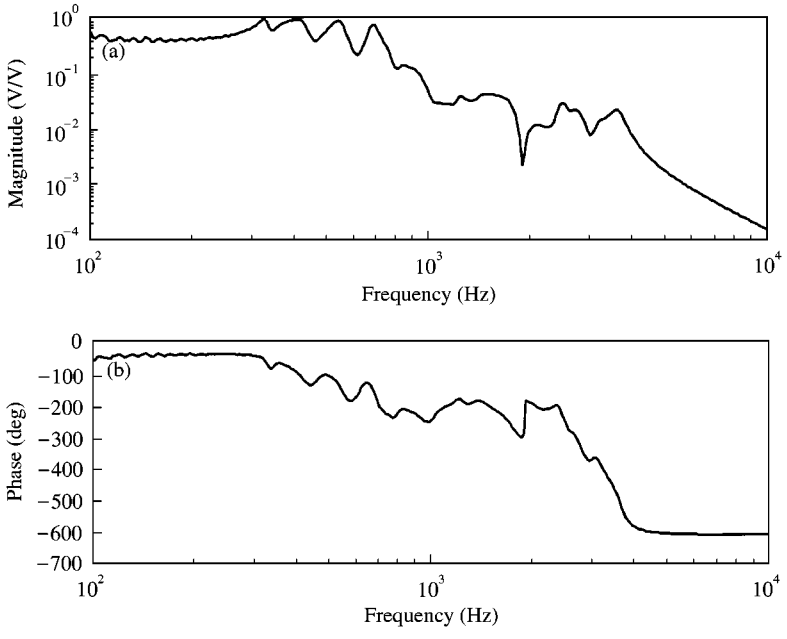

Figure 12. Loop-gain, $\mathbf{K}(s)\mathbf{P}_{yu}(s)$, of the system with compensator designed using the 1-D cavity model as the performance weighting filter.

[20]. The $\mathscr{H}_2$ norm of the frequency response of the closed-loop system from the modal disturbance input to the acoustic pressure performance metric, shown in Figure 13, is calculated from the sum of the squares of the singular values of each input/output path at each frequency [20]. As Figure 13 shows, the control system significantly reduces the contribution of the axial modes of the cylinder to the acoustic pressure within the cavity. The frequency responses of the open- and closed-loop systems from actuator to sensor are shown in Figure 14. The closed-loop system demonstrates reduction at the resonances of

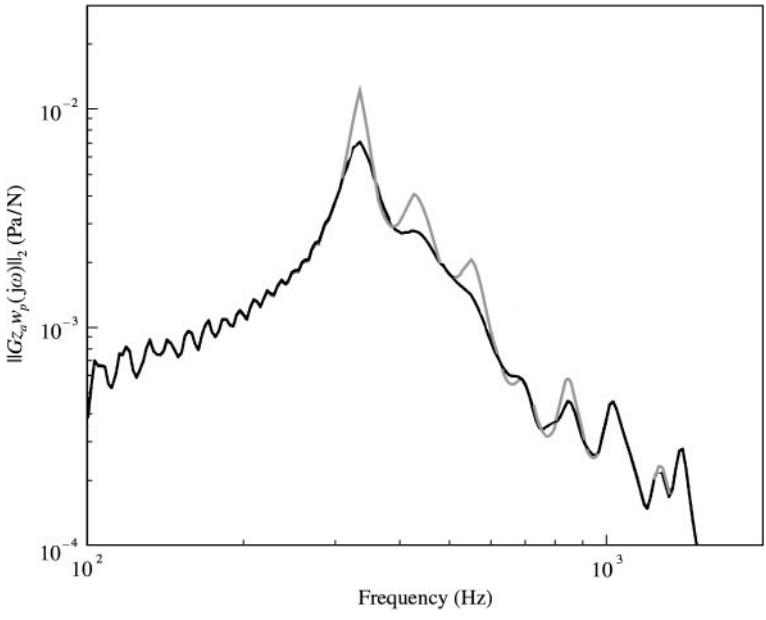

Figure 13. Frequency responses of open- and closed-loop systems from the modal disturbance to the acoustic performance, $\mathbf{w}_p(s)$ to $\mathbf{z}_a(s)$: – – – – –, open loop; ——, closed loop.

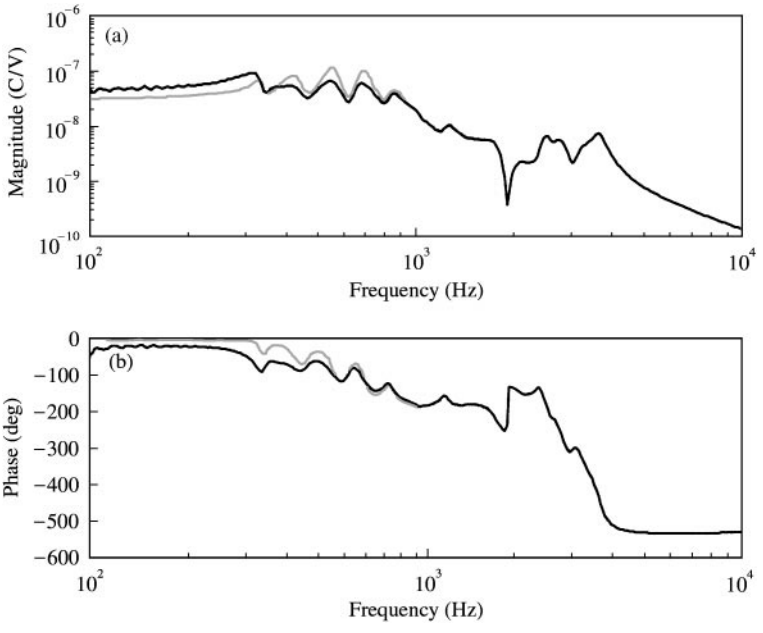

Figure 14. Frequency responses of open-loop ($P_{yu}(j\omega)$) and closed-loop ($T_{yu}(j\omega)$) systems from actuator to sensor: – – – – –, open loop; ——, closed loop.

the low order, axial modes of the panel, with no noticeable impact on modes with resonances above 1000 Hz. Figure 15 shows the frequency response of the closed-loop system from the augmented disturbance input, $\mathbf{w}_u(s)$, to the control input signal energy output, $\mathbf{z}_u(s)$. This response represents the ratio of the control input signal energy to the

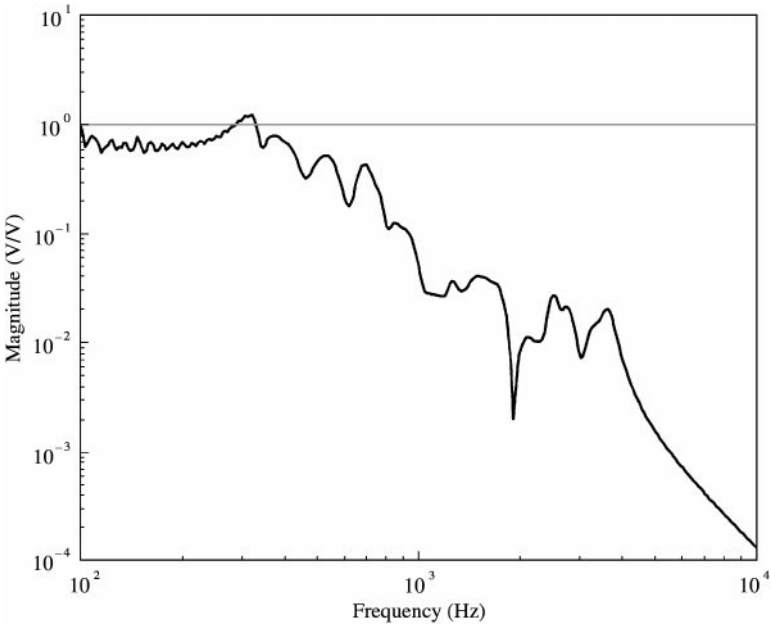

Figure 15. Ratio of control input signal energy to disturbance input signal energy.

disturbance input signal energy at each frequency, and provides a relative measure of the efficiency of the controller. When the ratio is less than unity, the signal energy required for control is less than the signal energy introduced through the control path by the disturbance and the controller is deemed efficient. When the ratio is greater than unity, more signal energy is required for control than is introduced by the disturbance. In this case, the ratio only exceeds unity at frequencies proximal to the resonance of the first structural mode, which is acceptable given the performance objectives of the controller.

In the second case, the compensator is designed utilizing as performance metrics the structural modal velocities weighted by the maximum structural acoustic coupling coefficient between each structural mode and the acoustic modes proximal in natural frequency. The sensor noise filter is defined as a constant gain filter with magnitude 7×10^{-8}, as previously discussed and shown in Figure 9. The control effort penalty filter is a constant gain filter with magnitude 1×10^{-8}. The performance weighting filter is defined such that the (1,1), (2,1), (3,1), (4,1), (1,2), and (5,1) structural modes are weighted according to the maximum normalized structural acoustic coupling coefficients listed in Table 1. All other structural modes are excluded from the performance metric. Figure 16 compares the frequency response of the generalized system from disturbance to performance with and without the performance weighting filter. The compensator design process yields the control law with frequency response show in Figure 17. The closed-loop system is formed as described above and shown in Figure 11. Figure 18 shows that the loop-gain, $\mathbf{K}(s)\,\mathbf{P}_{yu}(s)$, has magnitude not exceeding unity over all frequencies, guaranteeing closed-loop stability. The $\mathscr{H}_2$ norm of the frequency response of the closed-loop system from the modal disturbance to the acoustic pressure performance metric is shown in Figure 19. The controller achieves reduction of the contribution of the axial modes to the pressure in the cavity similar to that of the controller presented previously using the 1-D cavity model as the performance weighting filter. The frequency responses of the open- and closed-loop systems from actuator to sensor are shown in Figure 20. The closed-loop system again demonstrates

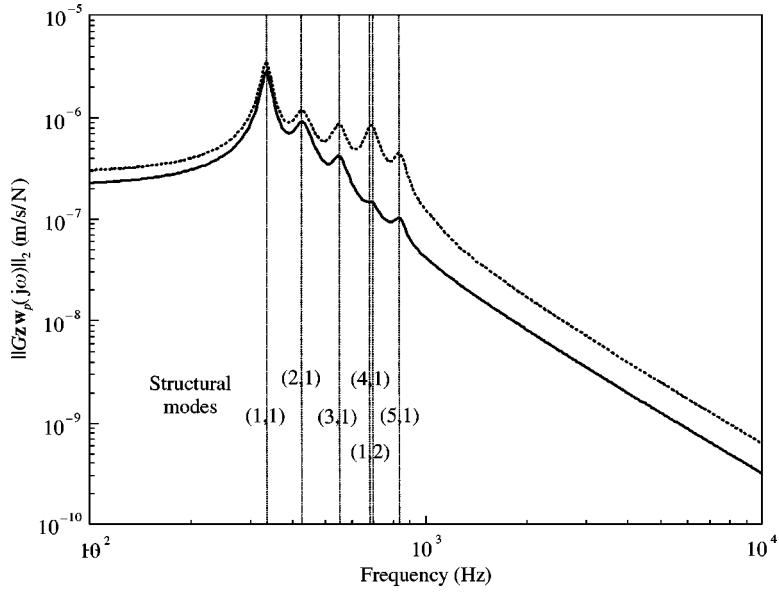

Figure 16. Comparison of weighted and unweighted frequency response of typical fuselage panel from the modal disturbance to the structural modal velocity performance metric, $\mathbf{w}_p(s)$ to $\mathbf{z}(s)$: – – – – –, unweighted; ——, weighted.

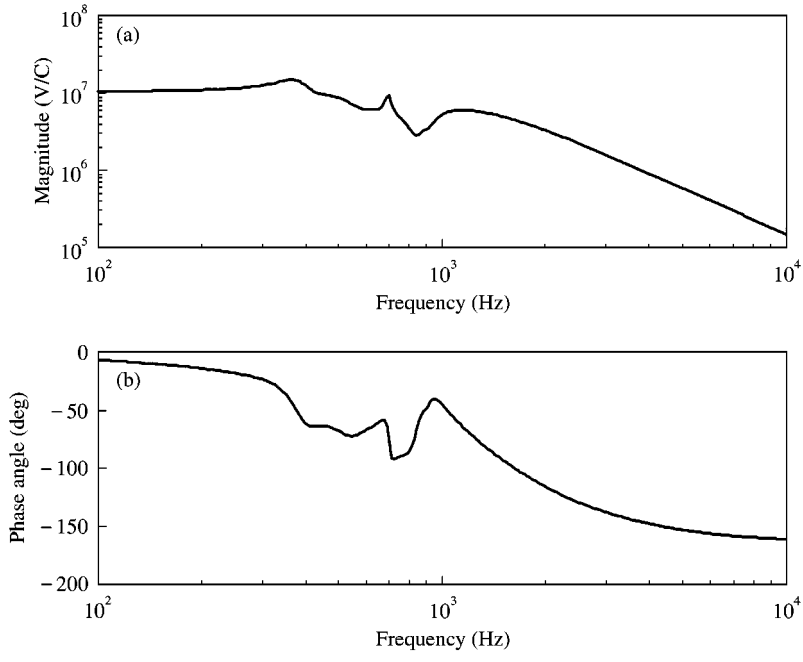

Figure 17. Frequency response of compensator designed using the structural acoustic coupling coefficients in the performance weighting filter.

reduction at the resonances of the low order, axial modes of the panel, with no noticeable impact on modes with resonances above 1000 Hz. Figure 21 shows the ratio of the control input signal energy to the disturbance input signal energy at each frequency. Again, the ratio only exceeds unity at frequencies proximal to the resonance of the first structural mode.

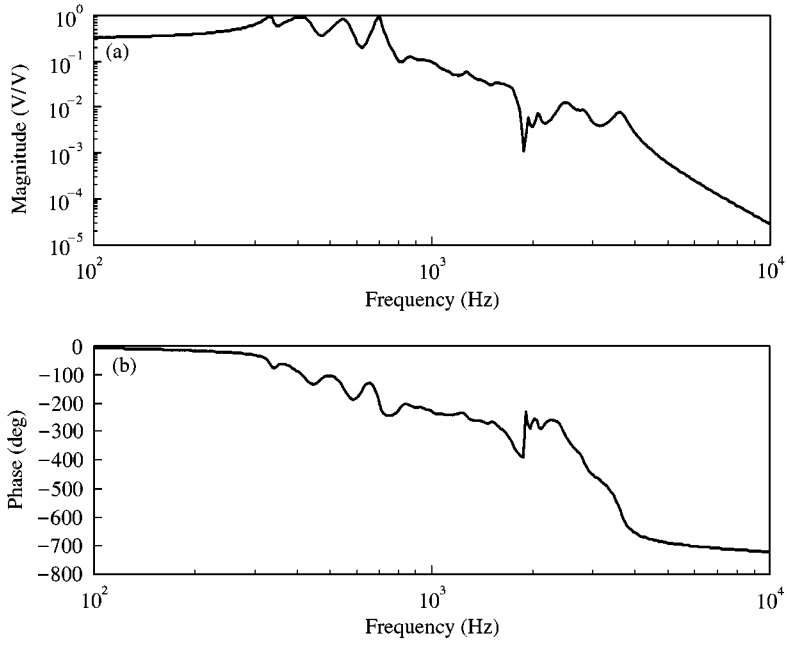

Figure 18. Loop-gain, $\mathbf{K}(s)\ \mathbf{P}_{yu}(s)$, of the system with compensator designed using the structural acoustic coupling coefficients in the performance weighting filter.

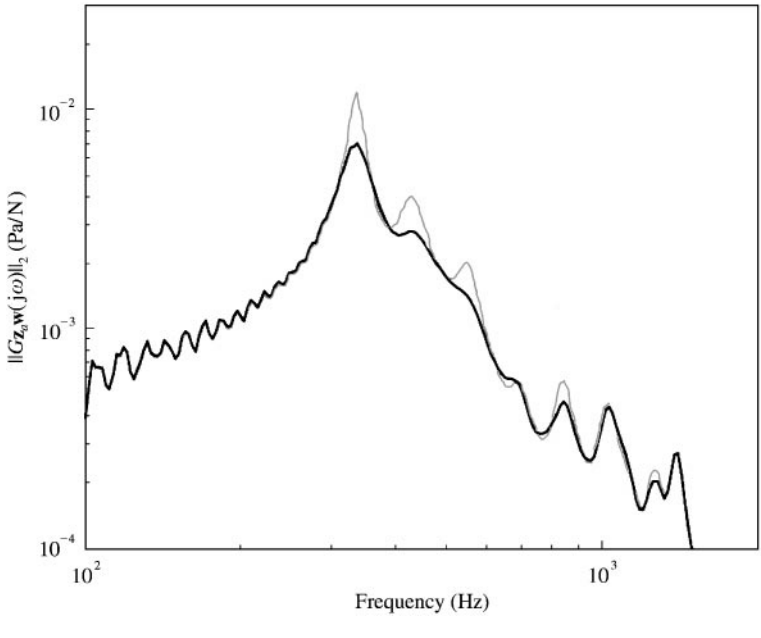

Figure 19. Frequency responses of open- and closed-loop systems from the modal disturbance to the acoustic performance metric, $\mathbf{w}_p(s)$ to $\mathbf{z}_a(s)$: -----, open loop; ——, closed loop.

As the closed-loop results indicate, the controller designed using a cost based on the structural acoustic coupling coefficients performs as well as the controller designed using a cost based on an estimate of the acoustic potential energy of the enclosure obtained from the 100 pressure measurements. These results show that it is possible to reduce the sound

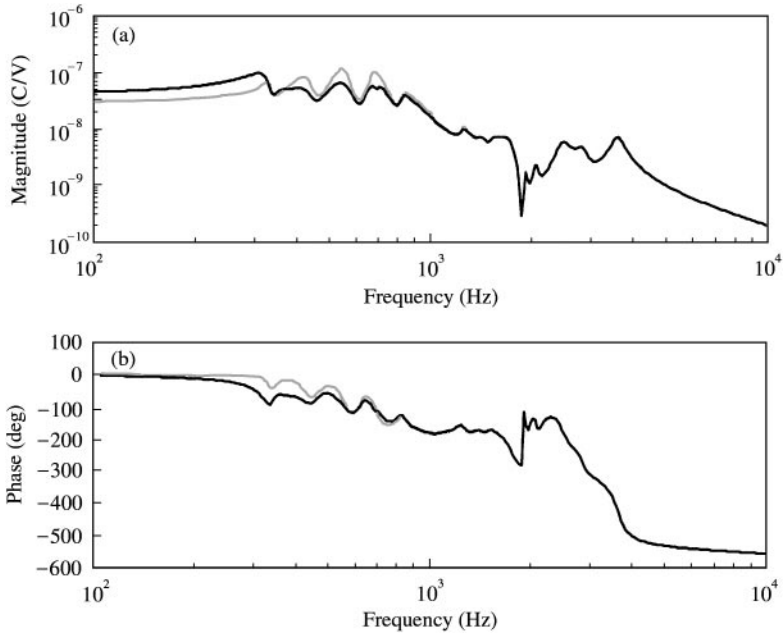

Figure 20. Frequency responses of open-loop ($P_{yu}(j\omega)$) and closed-loop ($T_{yu}(j\omega)$) systems from actuator to sensor: – – – – –, open loop; ——, closed loop.

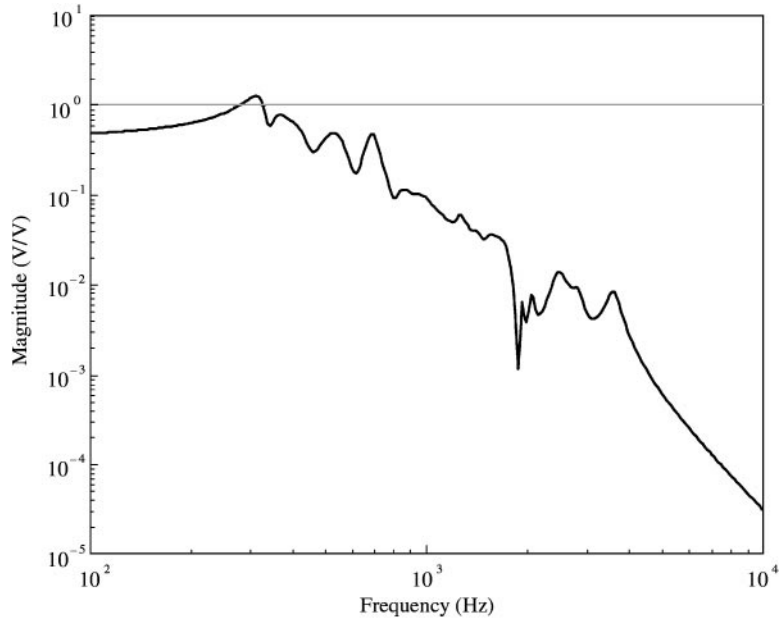

Figure 21. Ratio of control input signal energy to disturbance input signal energy.

transmission from the typical fuselage panel without measurements of the sound pressure within the cavity. Insight gained from the analysis of the structural acoustic coupling was vital to the design of the structural acoustic control system for reduction of the noise transmission from the panel into the enclosure. Additionally, using model reduction

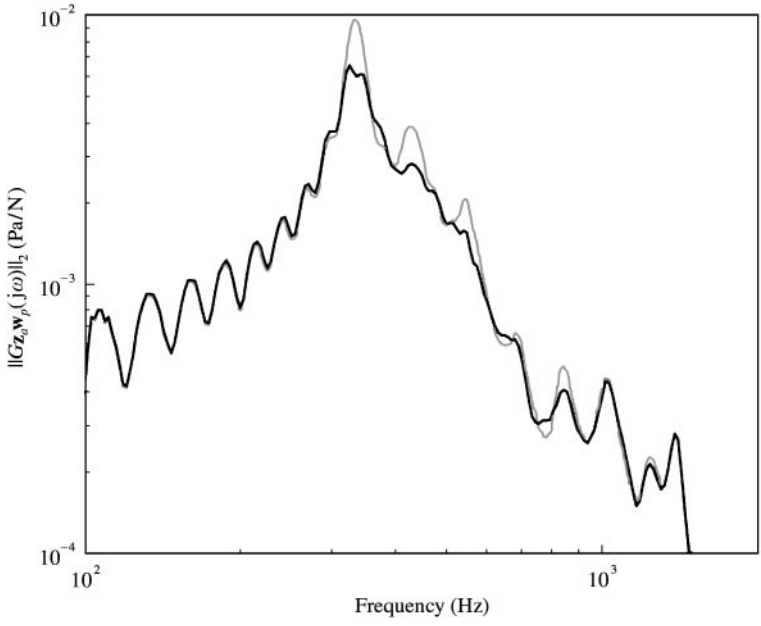

Figure 22. Frequency responses of open- and closed-loop systems from the modal disturbance to the acoustic performance for an "off-nominal" panel, $\mathbf{w}_p(s)$ to $\mathbf{z}_a(s)$: – – – – –, open loop; ——, closed loop.

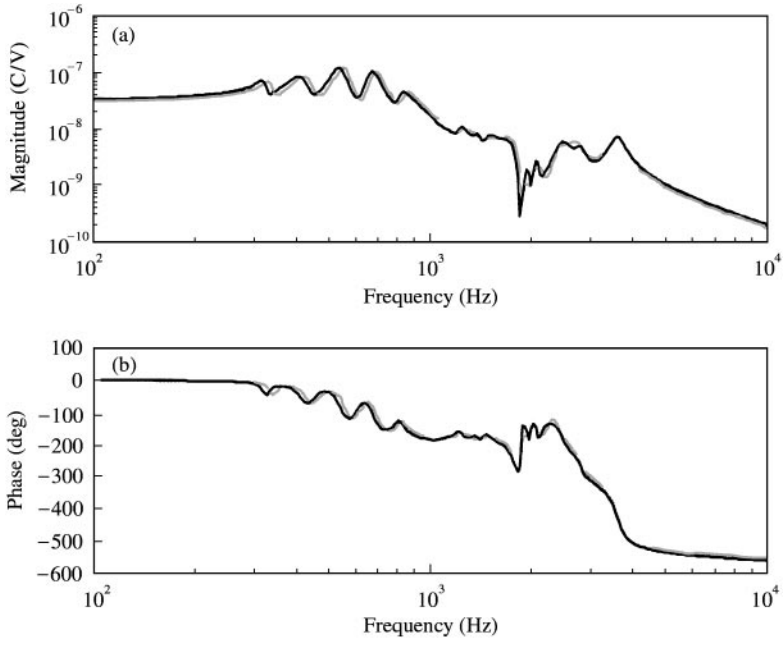

Figure 23. Comparison of open-loop ($P_{yu}(j\omega)$) frequency responses from actuator to sensor for small pressure perturbation: ------, altitude of 40 000 ft; ——, altitude of 35 000 ft.

techniques available in the μ-Analysis and Synthesis Toolbox [21], the order of the structural acoustic controller can be reduced to a fifth order control law without degradation of performance, for the case studied.

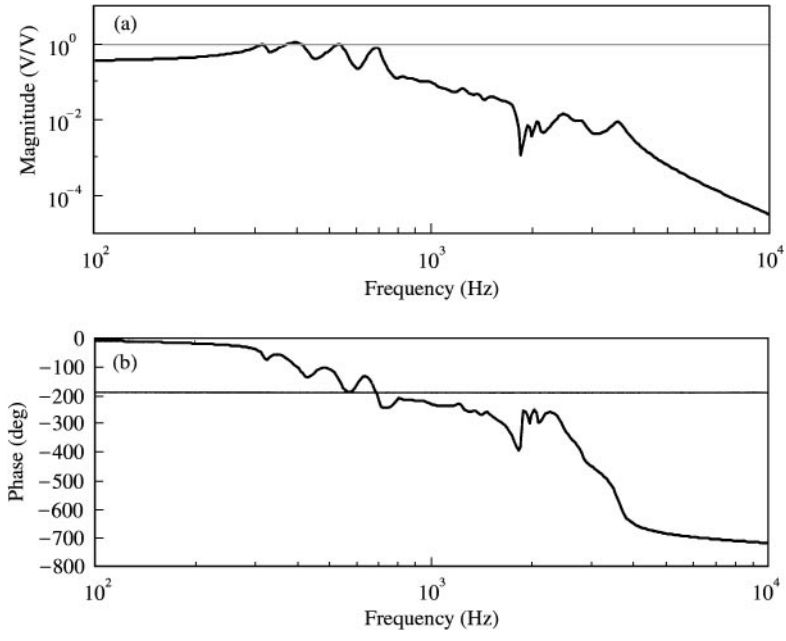

Figure 24. Loop-gain, $\mathbf{K}(s)\mathbf{P}_{yu}(s)$, of the system for small pressure perturbation.

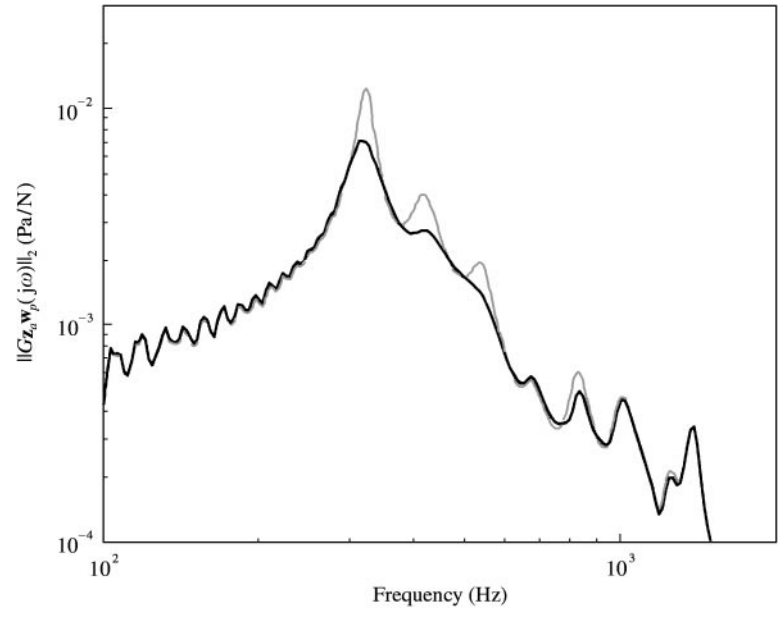

Figure 25. Frequency responses of open- and closed-loop systems from the modal disturbance to the acoustic performance, with small pressure perturbation: – – – – –, open loop; ——, closed loop.

6. VARIATIONS IN SYSTEM DYNAMICS

The control systems presented in the previous section are designed for a typical fuselage panel subjected to a prescribed static pressure load and based on the maximum structural

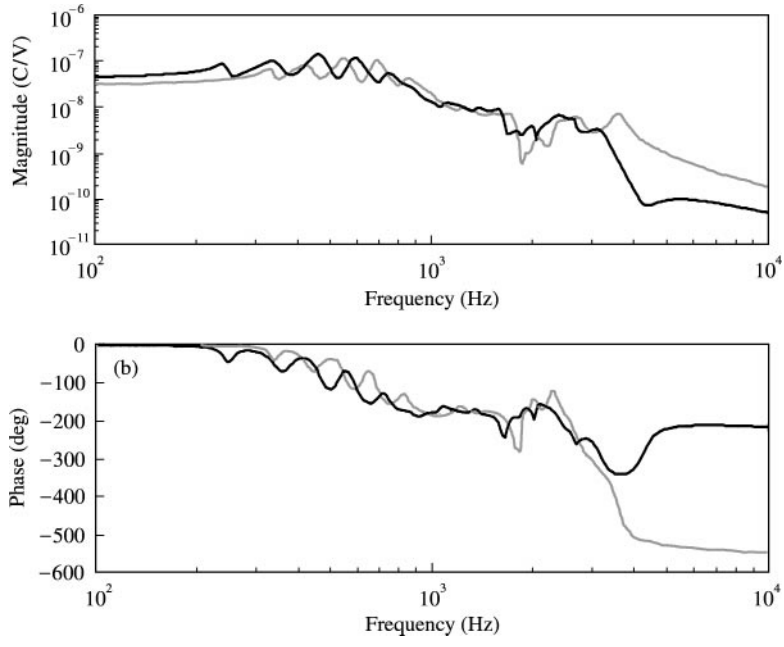

Figure 26. Comparison of the open-loop frequency responses from actuator to sensor for large pressure perturbation: -----, altitude of 40 000 ft; ——, altitude of 20000 ft.

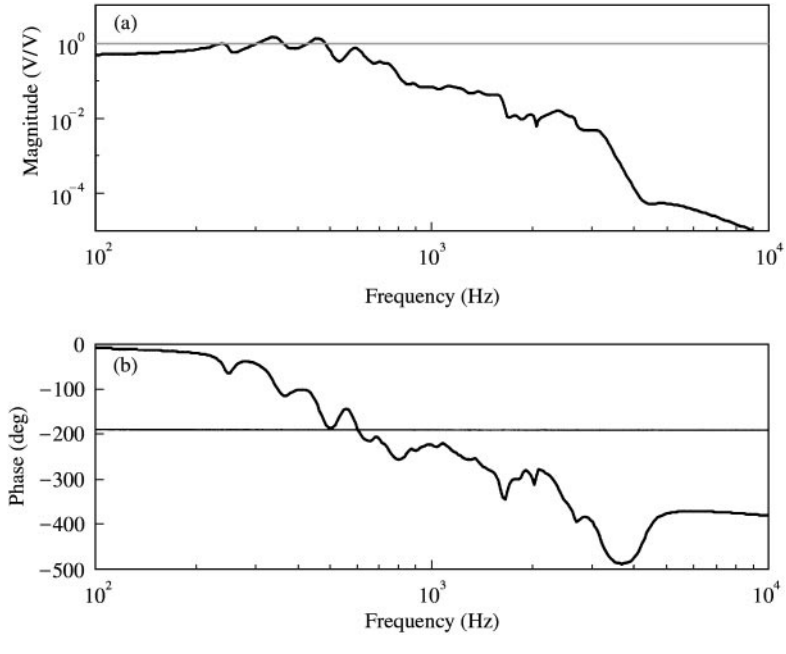

Figure 27. Loop-gain, $\mathbf{K}(s)\mathbf{P}_{yu}(s)$, of the system for large pressure perturbation.

acoustic coupling coefficients. For the control system to be implemented in practice, the same compensator must be able to be applied to each panel on the fuselage, regardless of position. Furthermore, the control system must be able to withstand variations in static pressure loading, and thus panel dynamics [16], with varying altitude without causing

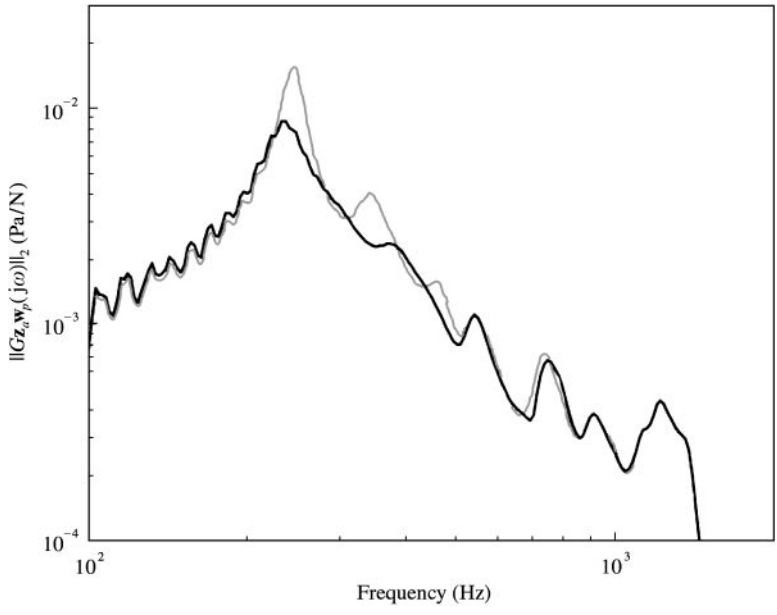

Figure 28. Frequency responses of open- and closed-loop systems from the modal disturbance to the acoustic performance, with large pressure perturbation: – – – – –, open loop; ——, closed loop.

instability. This section first examines the effectiveness of the control design on panels positioned elsewhere on the cylindrical enclosure. Then, the performance of the typical panel controller for varying static pressure loading is investigated.

6.1. VARIATION OF PANEL POSITION ON ENCLOSURE

Analysis of the structural acoustic coupling between the curved panel and the cylindrical enclosure established that panel position on the enclosure does not significantly affect the maximum coupling between the structural modes and the acoustic modes proximal in natural frequency [16]. Therefore, it follows intuitively that the controller design based on the structural acoustic coupling coefficients can be implemented regardless of panel position. In order to demonstrate this assertion, consider the typical fuselage panel now centered 45% down the length of the cylinder, such that $x_0 = 0{\cdot}45L_c - (L_x/2)$, and placed circumferentially starting at $\phi = 0$. The control design from the previous section based on the maximum structural acoustic coupling coefficients is applied to the panel at the new position. Since the dynamics of the panel are unaffected by the variation in position due to the insignificance of the acoustic pressure feedback path, the loop-gain of the system remains the same as shown in Figure 18. Thus, the control system is stable over all frequencies. Figure 22 shows the frequency response from the modal disturbance to the acoustic performance metric of the closed-loop system. Significant reduction of the contribution of the axial acoustic modes to the acoustic pressure in the cylinder is achieved. Similar results can be achieved at each panel position on the cylinder. Therefore, the control system designed can be implemented regardless of panel position on the cylinder. Furthermore, since the acoustic feedback path is negligible, the control systems can be operated independently.

6.2. VARIATION OF STATIC PRESSURE LOADING

Analysis has shown that the variation of panel dynamics with varying static pressure loading is significant [15]. Specifically, the natural frequencies of the structural modes vary substantially with large perturbations in pressure loading. The control system presented was designed based on the dynamics of a curved panel subjected to a static pressure load representative of that encountered by a fuselage panel at a cruise altitude of 40 000 ft. Ideally, the control system applied to the fuselage panels would be capable of performing at any altitude. However, given the significant variation in panel dynamics, it is not practical to expect that a controller designed for a particular pressure load is capable of achieving performance for all possible pressure loads. It is more realistic to demand that the control system achieve reduction for small perturbations in pressure loading and remain stable over all pressure loads.

Given this goal, consider a typical fuselage panel with the same dimensions and position as originally described, subjected to a static pressure load representative of that encountered by a fuselage panel at an altitude of 35 000 ft. Figure 23 compares the open-loop frequency responses from sensor to actuator of a curved panel subjected to the different static pressure loads. As the figure shows, the dynamics of the curved panel are only minorly affected by the small perturbation in static pressure loading. Implementing the previously designed controller on this system, it can be seen in Figure 24 that the magnitude of the loop-gain of the perturbed system barely exceeds unity at frequencies proximal to the resonances of the low order, axial structural modes. However, the phase at these frequencies is greater than -180°, guaranteeing closed-loop stability [20]. The frequency response of the closed-loop system from the modal disturbance to the acoustic performance, shown in Figure 25, indicates that the controller still achieves significant reduction of the contribution of the axial acoustic modes to the pressure within the enclosure. The control system is able to achieve performance despite minor perturbations in pressure loading.

Now, consider the same panel subjected to a static pressure load representative of that encountered by a fuselage panel at an altitude of 20 000 ft. Figure 26 indicates that the frequency response from sensor to actuator is significantly affected by the difference in static pressure loading. Implementing the previously designed controller on this curved panel, it can be seen in Figure 27 that the magnitude of loop-gain of the system exceeds unity in the proximity of several of the structural resonances. However, the phase of the loop-gain at the frequencies where the magnitude exceeds unity is greater than -180°. Therefore, the closed-loop system is stable over all frequencies [20]. The frequency response of the closed-loop system from the modal disturbance to the acoustic performance, shown in Figure 28, indicates that the system performance has been degraded, but that reduction is still achieved at several of the panel resonances. The proposed control design does not produce instability despite major perturbations in pressure loading.

The structural acoustic controller does not produce instability with variations in the panel dynamics since the fifth order control law is rather benign, resembling a low-pass filter (refer to Figure 17). Overall, the magnitude and phase required to achieve the desired control are relatively insensitive to the variations in the resonant frequencies of the panel. Specifically, the loop-gain of the system is always less than unity when the phase crosses -180°, regardless of the variations in pressure loading. This stems from the optimal spatial design of the piezoelectric transducers. Since the actuator to sensor path, shown for the various pressure loads in Figures 7, 23 and 26, is characterized by alternating complex conjugate pairs of poles and zeros over the desired control bandwidth, the phase does not cross -180° until higher frequencies. The compensator is designed to produce roll-off beyond the control bandwidth, causing the loop-gain of the system to be less than unity at

the higher frequencies where the phase is less than -180°. Therefore, the closed-loop system is stable, despite the variations in panel dynamics.

It may be possible to utilize gain scheduling techniques or adaptive control to maintain performance over all possible static pressure loads. The performance achieved by this control design will serve as a benchmark for future investigations of these potential solutions.

7. CONCLUSIONS

This work has established that active structural acoustic control through attached piezoelectric transducers can be used to reduce the sound transmission from typical fuselage panels into the interior of a cylindrical enclosure as a result of turbulent boundary layer excitation. Furthermore, this work has established that active structural acoustic control systems can be designed based only on the dynamics of the typical fuselage panel and knowledge of the structural acoustic coupling, obviating the need for a fully coupled model of the structural acoustic system. A simple, efficient method of including a structural acoustic performance metric based on the maximum structural acoustic coupling coefficients for each structural mode was presented. It was also shown that, since the same structural modes demonstrate significant coupling to the acoustic modes of the enclosure regardless of panel position on the cylinder, similar, independent active structural acoustic control systems designed based on the maximum structural acoustic coupling coefficients can be implemented on each panel on the fuselage. As a result of the optimal spatial design used, the control systems will at best achieve significant reduction to sound transmission despite small perturbations in pressure loading with varying flight altitude, and at least remain stable over all possible pressure loads.

ACKNOWLEDGMENT

This work was supported by NASA Langley Research Center under grant NCC 1 250.

REFERENCES

1. W. T. Baumann, W. R. Saunders and H. H. Robertshaw 1992 *Journal of the Acoustical Society of America* **92**, 1998–2005. Active structural acoustic control of broadband disturbances.
2. Yi Gu, R. L. Clark, C. R. Fuller and A. C. Zander 1994 *American Society of Mechanical Engineers Journal of Vibration and Acoustics* **116**, 303–308. Experiments on active control of plate vibration using piezoelectric actuators and polyvinylidene fluoride modal sensors.
3. R. L. Clark and C. R. Fuller 1992 *Journal of the Acoustical Society of America* **92**, 1521–1533. Optimal placement of piezoelectric actuators and polyvinylidene fluoride (PVDF) error sensors in active structural acoustic control approaches.
4. R. L. Clark and C. R. Fuller 1992 *Journal of Intelligent Material Systems and Structures* **3**, 296–315. Active structural acoustic control with adaptive structures and wavenumber considerations.
5. R. L. Clark and C. R. Fuller *Journal of the Acoustical Society of America* **91**, 3313–3320. Experiments on active control of structurally radiated sound using multiple piezoceramic actuators.
6. R. L. Clark and C. R. Fuller 1991 *Journal of Intelligent Material Systems and Structures* **2**, 431–452. Control of sound radiation with adaptive structures.
7. J. S. Vipperman and R. L. Clark 1997 *Journal of the Acoustical Society of America* **105**, 219–225. Multivariable feedback active structural acoustic control with adaptive piezoelectric sensoriactuators.

8. J. S. VIPPERMAN 1996 *Ph.D. thesis, Duke University*. Adaptive piezoelectric sensoriactuators for active structural acoustic control.
9. S. KOSHIGOE, J. T. GILLIS and E. T. FALANGAS 1993 *Journal of the Acoustical Society of America* **94**, 900–907. A new approach for active control of sound transmission through an elastic plate backed by a rectangular cavity.
10. K. D. FRAMPTON and R. L. CLARK 1997 *Proceedings of the* 38*th structures, structural dynamics and materials conference, Kissimee, FL*, April. Active control of noise transmission through an aeroelastic plate.
11. K. D. FRAMPTON and R. L. CLARK 1997 *Journal of the Acoustical Society of America* **102**, 1620. Power flow in an aeroelastic plate backed by a reverberant cavity.
12. K. D. FRAMPTON and R. L. CLARK 1997 *American Institute of Aeronautics and Astronautics Journal* **35**, 1113–1118. Sound transmission through an aeroelastic plate into a cavity.
13. K. D. FRAMPTON 1996 Active control of noise transmission through an aeroelastic plate into an acoustic enclosure. *Ph.D. thesis, Duke University*.
14. J. K. HENRY and R. L. CLARK 1999 *Journal of the Acoustical Society of America* **106**, 1400–1407. A curved piezo-structure model: implications on active structural acoustic control.
15. J. K. HENRY and R. L. CLARK 1999 *Proceedings of SPIE's* 6*th annual international symposium on smart structures and materials, Newport Beach, CA, Paper* 3668-09. Smart aircraft panels: the effects of internal pressure loading on panel dynamics.
16. J. K. HENRY and R. L. CLARK 1999 *Proceedings of active*'99: *the* 1999 *international symposium on active control of sound and vibration, Fort Lauderdale, FL*. Structural acoustic control of a cylindrical enclosure: analysis of structural acoustic coupling.
17. F. FAHY 1985 *Sound and Structural Vibration*. London: Academic Press.
18. R. L. CLARK and D. E. COX 1999 *American Institute of Aeronautics and Astronautics Journal of Guidance, Control, and Dynamics* **22**, 740–743. Band-limited actuator and sensor selection for disturbance rejection: application of structural acoustic control.
19. G. C. SMITH and R. L. CLARK 1999 *Proceedings of active*'99: *the* 1999 *international symposium on active control of sound and vibration, Fort Lauderdale, FL*. Adaptive structure design through optimum spatial compensation.
20. R. L. CLARK, G. P. GIBBS and W. R. SAUNDERS 1998 *Adaptive Structures, Dynamics and Control*. New York: John Wiley and Sons.
21. The Math Works, Inc. 1995 *MATLAB μ-Analysis and Synthesis Toolbox*.